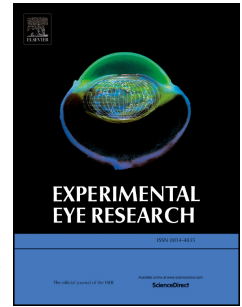


# Journal Pre-proof

Spectral domain - Optical coherence tomography (SD-OCT) as a monitoring tool for alterations in mouse lenses

Daniel Pawliczek, Claudia Dalke, Helmut Fuchs, Valerie Gailus-Durner, Martin Hrabě de Angelis, Jochen Graw, Oana Veronica Amarie



PII: S0014-4835(19)30592-5

DOI: <https://doi.org/10.1016/j.exer.2019.107871>

Reference: YEXER 107871

To appear in: *Experimental Eye Research*

Received Date: 8 August 2019

Revised Date: 8 October 2019

Accepted Date: 11 November 2019

Please cite this article as: Pawliczek, D., Dalke, C., Fuchs, H., Gailus-Durner, V., Hrabě de Angelis, M., Graw, J., Amarie, O.V., Spectral domain - Optical coherence tomography (SD-OCT) as a monitoring tool for alterations in mouse lenses, *Experimental Eye Research* (2019), doi: <https://doi.org/10.1016/j.exer.2019.107871>.

This is a PDF file of an article that has undergone enhancements after acceptance, such as the addition of a cover page and metadata, and formatting for readability, but it is not yet the definitive version of record. This version will undergo additional copyediting, typesetting and review before it is published in its final form, but we are providing this version to give early visibility of the article. Please note that, during the production process, errors may be discovered which could affect the content, and all legal disclaimers that apply to the journal pertain.

© 2019 Published by Elsevier Ltd.

# Spectral Domain - Optical Coherence Tomography (SD-OCT) as a Monitoring Tool for Alterations in Mouse Lenses

Daniel Pawliczek<sup>a,1</sup>, Claudia Dalke<sup>a,2</sup>, Helmut Fuchs<sup>b,3</sup>, Valerie Gailus-Durner<sup>b,4</sup>, Martin Hrabě de Angelis<sup>b,c,d,5</sup>, Jochen Graw<sup>a,6</sup>, Oana Veronica Amarie<sup>b,7,\*</sup>

<sup>a</sup>Helmholtz Zentrum München GmbH- German Research Center for Environmental Health, Institute of Developmental Genetics, Neuherberg, Germany

<sup>b</sup>Helmholtz Zentrum München GmbH - German Research Center for Environmental Health, Institute of Experimental Genetics, Neuherberg, Germany

<sup>c</sup>Chair of Experimental Genetics, School of Life Science Weihenstephan, Technische Universität München, Freising, Germany

<sup>d</sup>German Center for Diabetes Research (DZB), Neuherberg, Germany

## Abstract

The eye lens displays a variety of phenotypes in the wake of genetical modifications or environmental influences. Therefore, a high-resolution *in vivo* imaging method for the lens is desirable. Optical coherence tomography (OCT) has become a powerful imaging tool in ophthalmology, especially for retinal imaging in small animal models such as mice. Here, we demonstrate an optimized approach specifically for anterior eye segment imaging with spectral domain OCT (SD-OCT) on several known murine lens cataract mutants. Scheimpflug and histological section images on the same eye were used in parallel to assess the observed pathologies. With SD-OCT images, we obtained detailed information about the different alterations from the anterior to the posterior pole of the lens. This capability makes OCT a valuable high-resolution imaging modality for the anterior eye segment in mouse.

**Keywords:** Mouse, Eye lens, Cataracts, OCT, Scheimpflug imaging

## 1. Introduction

Optical coherence tomography (OCT) is used to produce high-resoluted, deep-reaching images of the retina and is now the standard for *in vivo* ophthalmological assessment [Huang et al., 1991] [Izatt et al., 2017]. It allows the non-invasive reconstruction of retinal tissue by light interference with near-histologic axial resolution. The incident infrared LASER-light penetrates the cornea, the anterior chamber, the entire lens and the vitreous,

in order to reach the retina. Therefore, every structure in front of the retina can be investigated. Anterior segment OCT (AS-OCT) was first demonstrated by Izatt et al. [1994]. The earliest commercial form of OCT was limited by relatively slow acquisition times and poor resolution. Later it was used by others mostly for imaging the anterior chamber angle in human patients [Asrani et al., 2008] [Fukuda et al., 2010] [Lavanya et al., 2008] [Nolan et al., 2007] [Radhakrishnan et al., 2001]. In more recent years a prototype of swept-source optical coherence tomography (SS-OCT) was employed to image human lenses from pole to pole [de Castro et al., 2018] [Grulkowski et al., 2018]. In mice, OCT was applied for biometrical purposes [Chou et al., 2011] [Zhou et al., 2008], with emphasis on the anterior lens and lens nucleus after deletion of *Glut1* in lenticular mouse epithelia [Swarup et al., 2018] and also for the lens nucleus and posterior lens [Liu et al., 2013].

\*Corresponding author

Email address:

oana-veronica.amarie@helmholtz-muenchen.de (Oana Veronica Amarie)

<sup>1</sup>ORCID:0000-0002-6682-8738

<sup>2</sup>ORCID:0000-0002-8040-4464

<sup>3</sup>ORCID:0000-0002-5143-2677

<sup>4</sup>ORCID:0000-0002-6076-0111

<sup>5</sup>ORCID:0000-0002-7898-2553

<sup>6</sup>ORCID:0000-0003-0298-9660

<sup>7</sup>ORCID:0000-0003-1705-6812

Another approach for the anterior eye segment imaging is the rotating Scheimpflug camera, a reliable tool for recording the entire human eye lens as well as the anterior and nuclear lens parts of common model organism as *Mus musculus*, *Rattus rattus* and *Oryctolagus cuniculus* [Wegener and Laser-Junga, 2009].

Pentacam<sup>®</sup> Scheimpflug device delivers quantitative information and qualitative imaging of the cornea and anterior chamber, as well as densitometry analysis of the lens opacification or cataract, based on reflectometry [Kim et al., 2009] [Pei et al., 2008]. Nevertheless, in mice it is not possible to apply Scheimpflug imaging to investigate the posterior eye lens, because of its rounder shape in comparison to the human lens.

Here, we demonstrate superior axial image resolution of SD-OCT as a preferred non-invasive mouse lens investigation method by using several already published mouse mutants with congenital and age-related lens alterations. SD-OCT images were assisted by AS-OCT, Scheimpflug and histology images with the aim to identify different lenticular pathological manifestations.

## 2. Materials and Supplies

### 2.1. Mice

At least three animals of nine different established mouse mutant lines and of one wild-type strain were examined (Tab. 1). The age at

Table 1: Mouse lines.

Mouse	Age	Reference
C57BL/6JG	10 wk.	MGI:6198736
<i>Crybb</i> <sup>O377/O377</sup>	12 wk.	[Ganguly et al., 2008]
<i>Crybb</i> <sup>2Philly/Philly</sup>	15 wk.	[Kador et al., 1980]
<i>Cryba</i> <sup>2Aca30/Aca30</sup>	6 wk.	[Puk et al., 2011]
<i>Crybb</i> <sup>2Aey2/Aey2</sup>	6 wk.	[Graw et al., 2001b]
<i>Crygd</i> <sup>Aey4/Aey4</sup>	16 wk.	[Graw et al., 2002]
<i>Cryaa</i> <sup>Aey7/Aey7</sup>	16 wk.	[Graw et al., 2001a]
<i>Pax6</i> <sup>+ /Aey11</sup>	20 wk.	[Graw et al., 2005]
<i>Ercc</i> <sup>2<sup>+</sup>/S737P</sup>	78 wk.	[Kunze et al., 2015]
<i>Ercc</i> <sup>2<sup>S737P</sup>/S737P</sup>	8 wk.	[Kunze et al., 2015]

All mice were bred on C57BL/6JG background with exception of *Crygd*<sup>Aey4/Aey4</sup>, *Cryaa*<sup>Aey7/Aey7</sup> and *Ercc*<sup>2<sup>S737P</sup>/S737P</sup> (C3HeB/FeJ) as well as the *Ercc*<sup>2<sup>+</sup>/S737P</sup> mutant (C57BL/6JG x C3HeB/FeJ)F1.

investigation of the mice was frequently higher than in the respective publications (with exception of *Crybb*<sup>2Aey2/Aey2</sup>) to cover all degrees of cataract severity.

All mice were housed in the animal facilities of the German Mouse Clinic (GMC, <https://www.mouseclinic.de>) in accordance with the German Law of Animal Protection, the ARVO Statement for the Use of Animals in Ophthalmic and Vision Research, and the tenets of the Declaration of Helsinki. All mice were examined with the permission of the Government of Upper Bavaria under ROB-55.2-2532.Vet.02-16-80.

In sequence, the mice were measured first with Scheimpflug, then with OCT and eventually sacrificed for histology.

### 2.2. Scheimpflug imaging

Lens opacity was analysed using the Scheimpflug (SP) system Pentacam<sup>®</sup> (Oculus GmbH, Wetzlar, Germany) according to Puk et al. 2009. Mydriasis was induced by 0.5% Atropin drops to allow optimal visualization of the lens. The mice were not anaesthetized and therefore not prone to cold cataracts or eye dehydration [Bermudez et al., 2011].

### 2.3. Optical coherence tomography (OCT)

Optical Coherence Tomography was performed with the Spectralis<sup>®</sup> OCT (Heidelberg Engineering, Heidelberg, Germany) as described by Puk et al. 2013. The technical requirements in brief were as follows: a 78-diopter double aspheric lens (Volk Optical, Inc., Mentor, OH, USA) was directly fixed on the optical outlet of the device. A second plan-convex contact lens (Roland Consult, Brandenburg, Germany) was reversibly attached to the eyes of the mice with contact medium (Methocel 2%, OmniVision, Puchheim, Germany). Mice were anaesthetised with ketamine (100 mg/kg)/xylazine (10 mg/kg).

### 2.4. Histology

After OCT and SP investigations, the mice were directly sacrificed, the enucleated eyes were fixed in Davidson and subsequently embedded in Technovit<sup>®</sup> 8100 (Heraeus Kulzer, Wehrheim, Germany). Samples were cut in 2 µm mid-sagittal sections with a glass knife ultramicrotome (OM U 3, C. Reichert, Austria) on superfrost slides and stained with basic fuchsin and methylene blue. Slides

were scanned (NanoZoomer S210 Digital slide scanner, Hamamatsu, Japan) and images taken with 10x, 20x and 40x objectives and processed with an image-processing program (GIMP 2.8.2, 2017, The GIMP team).

### 3. Detailed OCT method: software and device settings

For OCT image acquisition, we recorded first AS-OCT images. The camera was positioned close to the eye, until the pupil was in focus on the live infrared (IR) frame. At this point, the camera head was fixed and by using the reference arm slider, the cornea and the lens reflection image were moved to the sweet spot of the AS-OCT acquisition window. The focus in all measurements was unchanged around 0 diopters (D). Cross-sectional images and volume scans through the anterior eye segment were recorded.

The next module measurement required the exchange of the lens at the output of the detection head for the OCT2 module lens. Additionally, a contact lens was applied to the eye of the mouse with a drop of Methocel. After changing to the spectral domain mode, the region of interest in the mouse lens could be fixed by OCT device slide readjustments. The focus was adjustable in principle and could be fine-tuned for different diopters, but in our hands only a focus around 0 D ensured contorted images in 1:1 scale, with the exception of an old *Ercc2<sup>+/S737P</sup>* mouse (10.75 D).

Automatic real-time tracking (ART) mode was used to achieve improved signal-to-noise ratio by averaging up to 100 image frames. Preference was given to volume scans of the entire central lens, when the mice were breathing calmly under anaesthesia. Images for this paper were displayed with enhanced contrast (level 14).

In this configuration, OCT imaging revealed lens matrix features that were not visible with the Scheimpflug method or even histology images.

## 4. Results

With focus on lens, it was possible with OCT measurements to detect *in vivo* and time-resolved a broad spectrum of specific fine structures.

### 4.1. OCT of anterior lens cortex and nucleus

A good example for the imaging of the anterior fine-structure of an altered eye lens was given

by the *Pax6<sup>+/Aey11</sup>* mutant. As a result of the mutation-induced developmental failure, a keratolenticular adhesion occurred (Fig. 1, C+D). This alteration was clearly depicted in SD-OCT (Fig. 1, A), whereas with the Scheimpflug camera examination, no clear statement concerning the exaggerated corneal reflection could be made (Fig. 1, B). Low-signal areas in the SD-OCT-depicted adhesion were most likely due to capsule invagination into the cornea (Fig. 1, D, red star), while increased signal areas were possibly caused by the locally hypertrophic lens epithelium (Fig. 1, D, black arrowheads). Additional scattering in the vicinity of the adhesion (Fig. 1, A, blue arrow) was caused possibly by granular cytoplasm of the fibre cells or by fibre cells with nuclei (Fig. 1, E, black arrowheads). AS-OCT of the eye displayed increased scattering too (Fig. 2, A), but was less sensitive to elucidate deeper structures of the lens, than SD-OCT, as visible in Fig. 1, A.

The next example, the *Crygd<sup>Aey4/Aey4</sup>* mutant eye contained a cataractous lens, which was observed as massive light scattering in the Scheimpflug image (Fig. 1, G), although overall histology of the eye revealed no obvious morphological changes (Fig. 1, H). Magnifications disclosed fibre cells with remnant nuclei or unknown aggregation located at the interface of lens cortex and nucleus (Fig. 1, J, black arrowheads). These spots were sufficiently detected by SD-OCT as increased large scattering zones in the lens nucleus (Fig. 1, F, blue arrows). The AS-OCT added no further information (Fig. 2, B) and offered less precise images of the anterior lens and nucleus than SD-OCT (e.g. anterior suture).

The cataractous lenses of the *Crybb2* mutants *Crybb2<sup>O377/O377</sup>* and *Crybb2<sup>Philly/Philly</sup>* (Fig. 3, C+H) were imaged with the Scheimpflug camera as undifferentiated blots due to total light scattering inside the lenses (Fig. 3, B+G).

The SD-OCT imaged not only almost the entire lenses, but revealed also with great accuracy the inner texture of the lenses in both mutants (Fig. 3, A+F) with near histological resolution. While in the Scheimpflug image of *Crybb2<sup>O377/O377</sup>* a signal-free area was partially visible (Fig. 3, B, red arrow), the SD-OCT image displayed the existing caverns lateral and posterior in the lens (Fig. 3, A, red arrows; Volume scan in supplemental data). The SD-OCT properly depicted even the thickened capsule of *Crybb2<sup>O377/O377</sup>* and *Crybb2<sup>Philly/Philly</sup>*

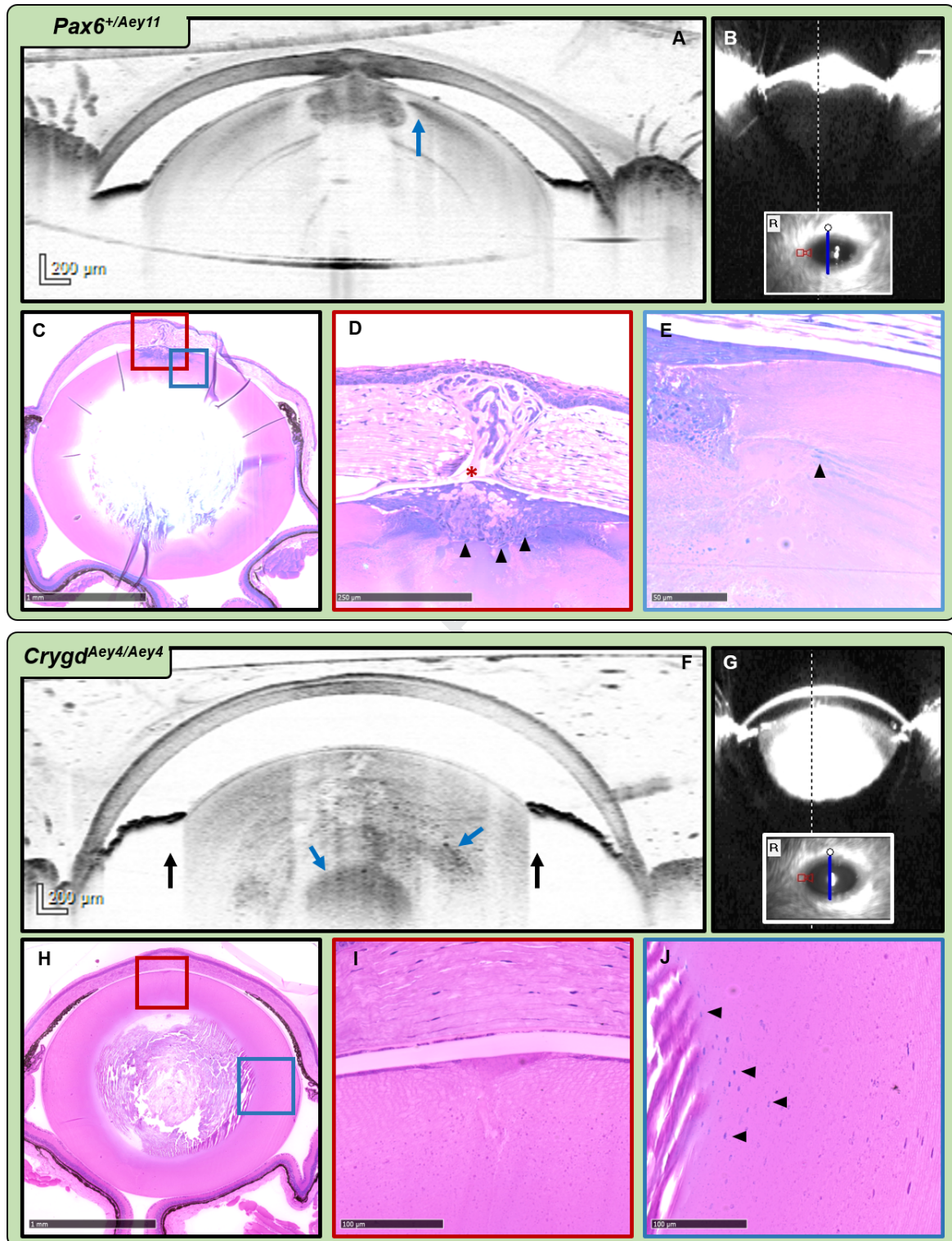


Figure 1: 20 weeks old *Pax6<sup>+/Aey11</sup>* (A-E) and 16 weeks old *Crygd<sup>Aey4/Aey4</sup>* (F-J) mutant: **A+F**. SD-OCT images of anterior lens. **B+G**. Scheimpflug images with small frontal picture. **C+H**. Histology of entire eye lens. **D+E+I+J**. Magnifications marked in overview images. (←) Iris-dependent signal cut-off of eccentric ventral lens extensions. (←) Scattering areas. (◄) Nuclei of epithelial cells or fibre cells. (\*) Lens capsule.

(Fig. 3, A+D+E+I, red stars). Lens detection with the anterior segment module contributed no more information and produced less sharp lens images (Fig. 2, C+D).

#### 4.2. OCT of lens nucleus

The *Crybb2<sup>Aey2</sup>* mutant lens was characterised by undifferentiated lens fibre cells, still carrying nuclei (Fig. 4, D, black arrowheads). Those nuclei of a failed lens epithelial cell differentiation were hardly visible in the outer cortex and not in the lens bow in SD-OCT (Fig. 4, A, blue arrows). Additionally, SD-OCT revealed a stratification of different light-scattering layers in the nucleus. A high-scattering outer nucleus was sharply distinguishable from a low-scattering inner nucleus (Fig. 4, A), whilst Scheimpflug imaging displayed no differences, but an utterly opaque appearance of the lens (Fig. 4, B).

In the *Cryba2* mutant *Aca30*, waves of scattering centres through the entire lens nucleus were detected in detail with SD-OCT (Fig. 4, F, blue arrows; Volume scan in supplemental data). The strong and intense OCT signal was not fully supported by the histology (Fig. 4, H), where fibre cells with nuclei were only discernible between the lens bow and the anterior lens part (Fig. 4, I+J), matching the appearance in the SD-OCT image. The signal did not match between lens bow and lens nucleus. In the Scheimpflug image, a slightly increased scattering at the lens bow and a cataractous alteration in the nucleus was detectable. The revealed nuclear alteration was consistent with the defect in the SD-OCT image (Fig. 4, G, blue arrow).

#### 4.3. OCT of posterior lens

Aside from the anterior and nuclear segment of the lens, the SD-OCT delivered the most detailed information about the posterior segment, as demonstrated for the *Cryaa* mutant *Aey7* and the heterozygous and homozygous *Ercc2* mutants. The *Cryaa* mutant *Aey7* was characterised by caverns in the equatorial and moreover in the posterior cortex (Fig. 5, D+E+F). The SD-OCT of the anterior segment revealed an increased occurrence of scattering layers as well (Fig. 5, A, blue arrow) which were not clearly distinguishable in the histology but seemed to mark the interface of fixed and non completely fixed lens areas (Fig. 5, D). Those scattering layers were most likely

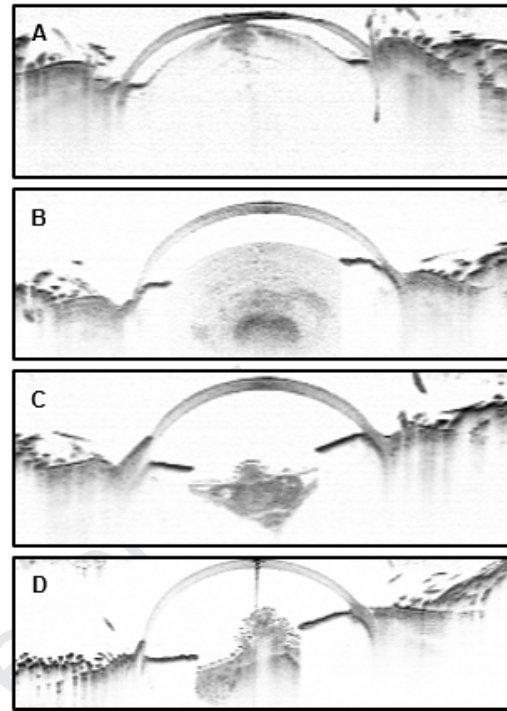


Figure 2: AS-OCT images of 20 weeks old *Pax6<sup>+</sup>/Aey11* (A), 16 weeks old *Crygd<sup>Aey4/Aey4</sup>* (B), 12 weeks old *Crybb2<sup>O377/O377</sup>* (C) and a 15 weeks old *Crybb2<sup>Philly/Philly</sup>* (D).

responsible for the appearance of a total cataract in the Scheimpflug image (Fig. 5, B). Obviously, the Scheimpflug camera was also limited in detecting the mainly posterior aggregated caverns. By contrast, the SD-OCT image of the posterior lens detected those caverns as signal-free areas (Fig. 5, C, red arrows).

The DNA repair-deficient mutant *Ercc2<sup>S737P/S737P</sup>* developed the well-documented nuclear cataract that was clearly visible in the Scheimpflug image (Fig. 5, H). In histology, the mutant displayed also ruptures or separations of the lens fibres in the anterior and posterior segment (Fig 5, J+K+L, red arrowheads). The anterior defects were fairly visible in the Scheimpflug image (Fig. 5, H, blue arrow), but not the posterior alterations. The SD-OCT images showed fibre cells with dens material that seems to accumulate towards the lens nucleus and displays also signal-free areas that indicate a change in lens matrix denseness (Fig. 5, G+I, blue arrow).

The aged *Ercc2<sup>+/S737P</sup>* mice displayed a ho-

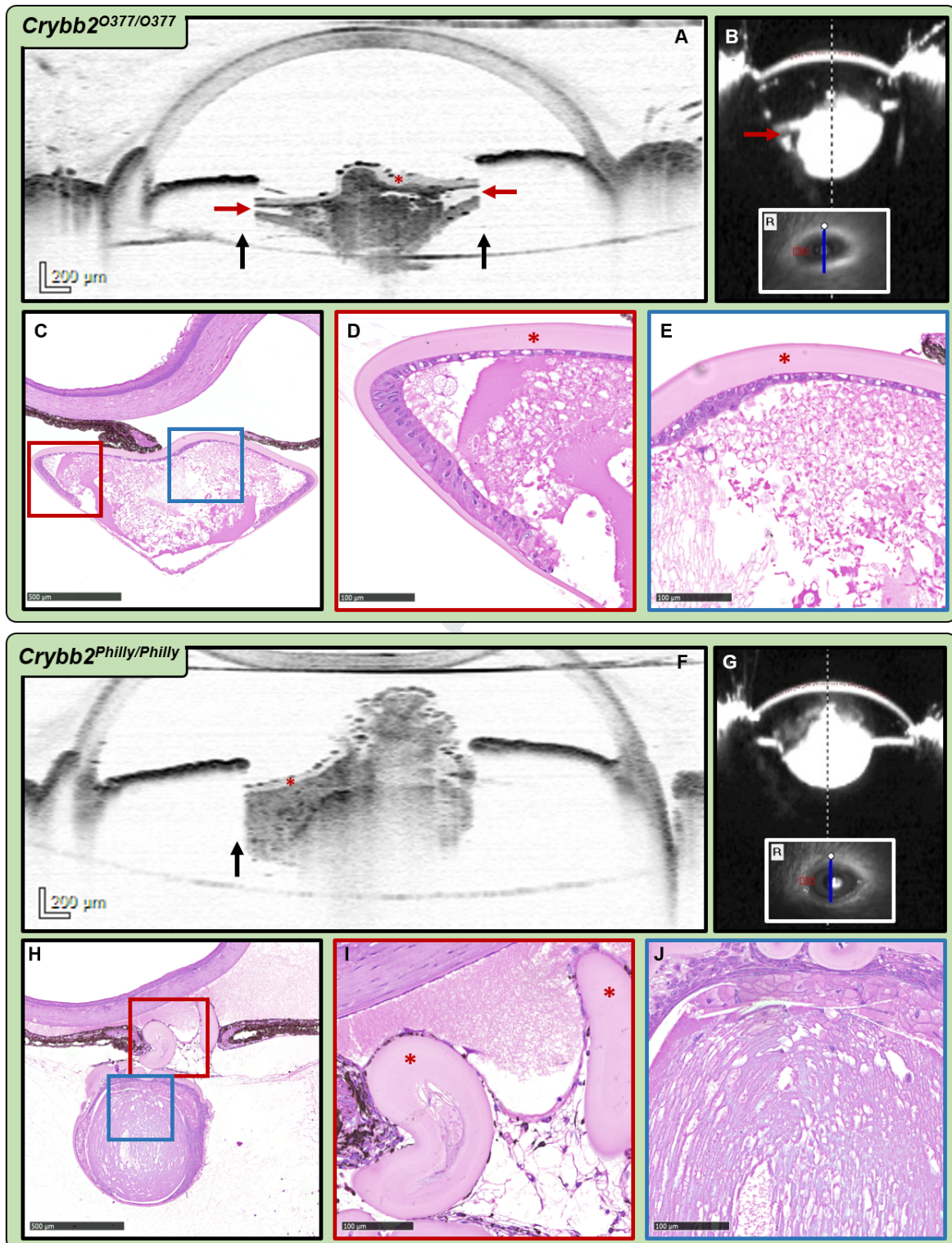


Figure 3: 12 weeks old *Crybb2*<sup>O377/O377</sup> (A-E) and 15 weeks old *Crybb2*<sup>Philly/Philly</sup> (F-J) mutant: **A+F**. SD-OCT images of entire lens. **B+G**. Scheimpflug images with small frontal picture. **C+H**. Histology of entire eye lens. **D+E+I+J**. Magnifications marked in overview images. ( $\leftarrow$ ) Iris-dependent signal cut-off of eccentric ventral lens extensions. ( $\leftarrow$ ) Caverns in the lens. (\*) Lens capsule.

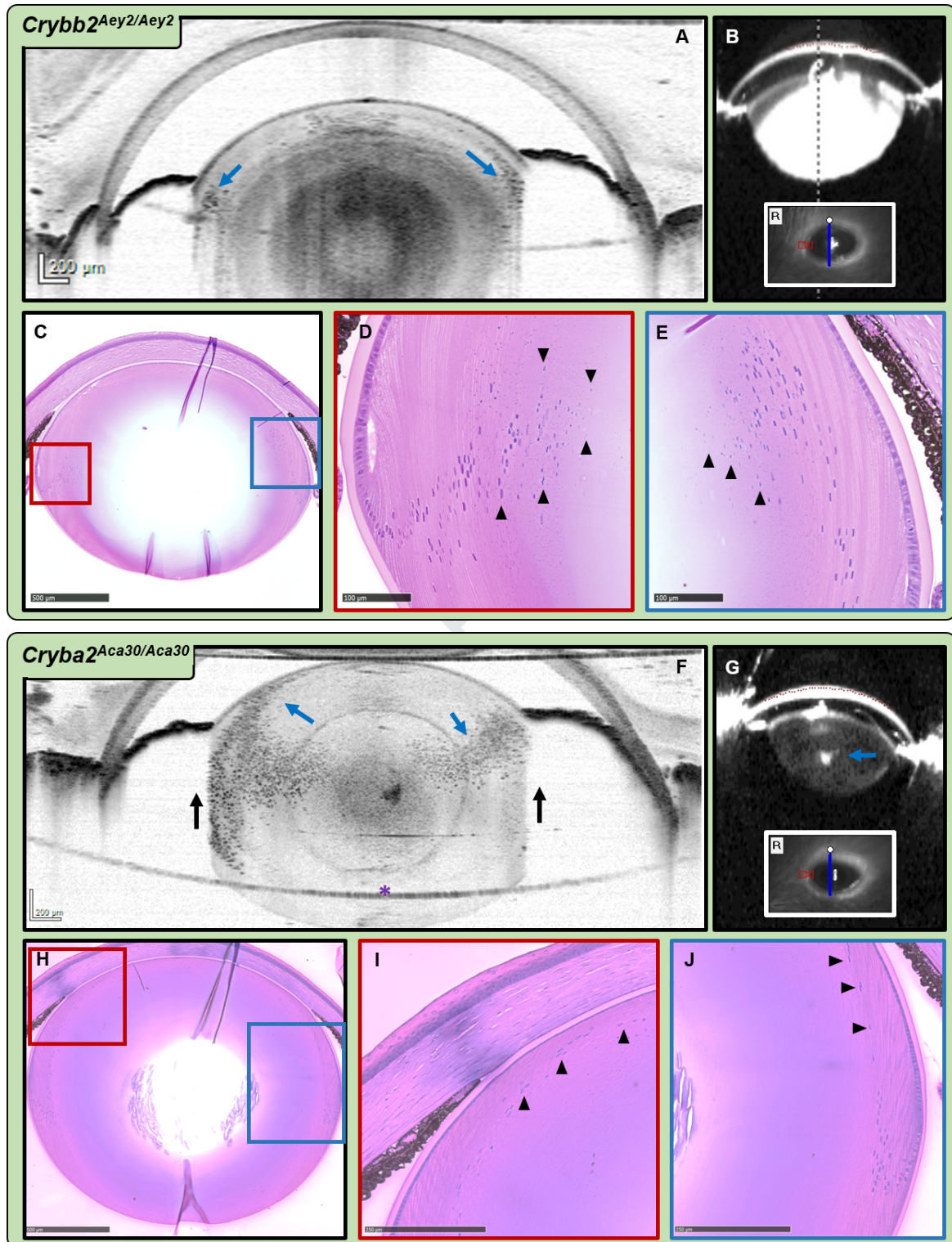


Figure 4: 6 weeks old *Crybb2<sup>Aey2/Aey2</sup>* (A-E) and 6 weeks old *Cryba2<sup>Aca30/Aca30</sup>* (F-J) mutants: **A+F**. SD-OCT images of entire lens. **B+G**. Scheimpflug images with small frontal pictures. **C+H**. Histology of entire eye lens. **D+E+I+J**. Magnifications marked in overview images. (←) Iris-dependent singal cut-off. (←) Puntiform scattering centre. (▲) Nuclei of fibre cells. (\*) Mirroring contact lens.

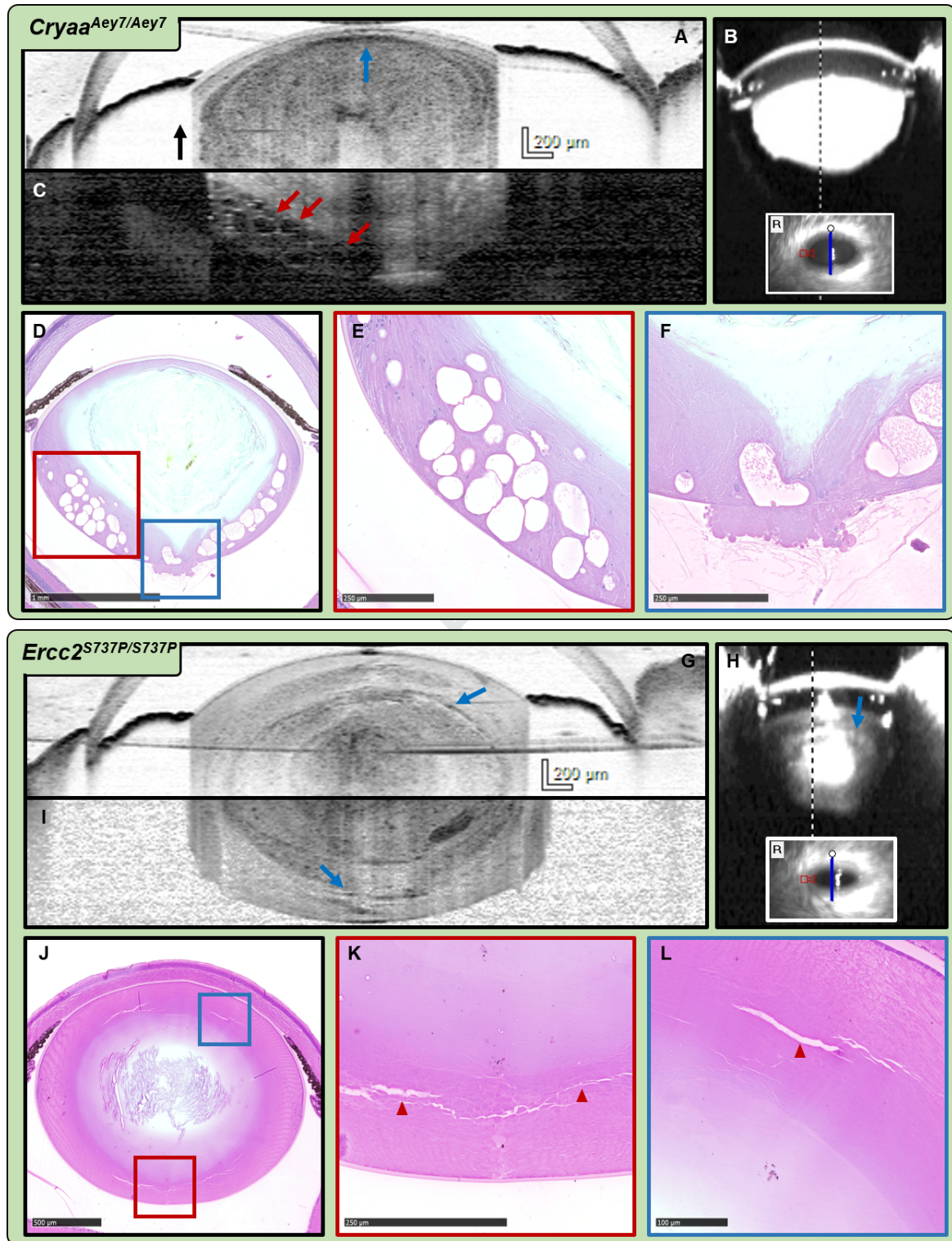


Figure 5: 16 weeks old *Cryaa<sup>Aey7/Aey7</sup>* (A-F) and 8 weeks old *Ercc2<sup>S737P/S737P</sup>* (G-L) mutants: **A+C+G+I**. SD-OCT images of anterior and central lens parts (C in white on black for better contrast). **B+H**. Scheimpflug images with small frontal picture. **D+J**. Histology of entire eye lens. **E+F+K+L**. Magnifications marked in overview images. (←) Iris-dependent signal cut-off of eccentric ventral lens extensions. (←) Signal-free planes in the lens. (←) Area of increased scattering. (◄) Disruptions in the lens.

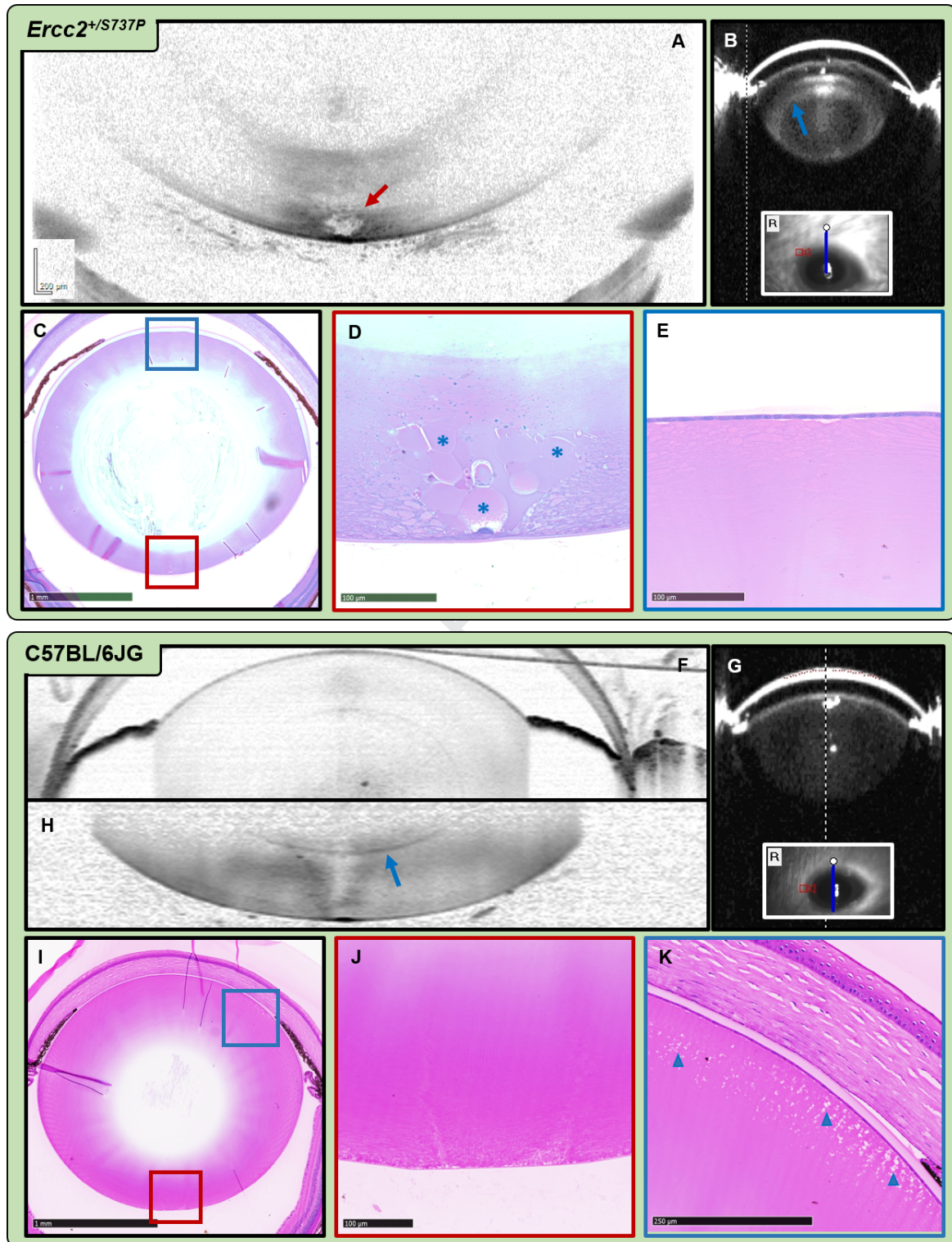


Figure 6: 78 weeks old *Ercc2*<sup>+/S737P</sup> mutant (A-E) and 10 weeks old *C57BL/6JG* control (F-K): **A+F+H**. SD-OCT images of posterior lens. **B+G**. Scheimpflug images with small frontal picture. **C+I**. Histology of entire eye lens. **D+E+J+K**. Magnifications marked in overview images. (←) Signal-free plane in the lens. (←) Cortex to nucleus interface scattering. (\*) Deposits or swollen fibre cells. (▲) Small vacuoles.

mogenously increased opacification at the interface of cortex and nucleus visible with Scheimpflug imaging (Fig. 6, B, blue arrow). This feature was age-related, as described in a previous study [Dalke et al., 2018] and evident at the microscopic level as a transition to the incompletely fixed and therefore poorly stained lens area (Fig. 6, C). However, the posterior cortex displayed a visible alteration in the histological section with the shape of a lesion at the posterior suture (Fig. 6, D, blue stars). The lesion was composed of large fibre cells and deposits respectively, enclosed by relatively regular-sized fibre cells out of typical fibre cell arrangement. This lesion was clearly detectable with the SD-OCT as a contrast of a signal-free area surrounded by increased light-scattering structures (Fig. 6, A, red arrow), but definitely not possible to image with the Scheimpflug camera.

The last example was a 10-week-old C57BL/6JG control mouse that had neither lens opacifications visible in the Scheimpflug image (Fig. 6, G), nor did the SD-OCT reveal any pathological alterations (Fig. 6, F). Only the scattering in the inner posterior cortex (blue arrow) was detectable (compare with Chou et al. 2011 in a later stage) but this feature had no obvious correlate in histology (Fig. 6, I). The posterior suture was clear in SD-OCT, which was confirmed by the histology of the specific area (suture bifurcation, Fig. 6, J). Despite being a control without expected lens alterations at this stage, histology revealed the occurrence of many vacuoles within or between fibre cells anteriorly to the lens bow (Fig. 6, K, blue arrowheads). Those vacuoles were not identified by SD-OCT, most likely because of lacking scattering substrate in and around the vacuole.

## 5. Potential pitfalls and troubleshooting

Undoubtedly, SD-OCT provided the high resolution for *in vivo* detection of mouse lens alterations and was successful for small animal imaging. At the same time, OCT was nonetheless confined, in our experiments, by natural limits such as the iris condition/opening, the lens size, the mouse age in general and structural signal interferences. Furthermore, opacification-free corneae or corneae with a limited opaque spot (as in *Aey11*) were obligatory for high resolution imaging.

### 5.1. Iris condition

The melanin-containing iris, which hampered the imaging of the whole eye lens in Scheimpflug imaging, cut off also eccentric equatorial parts of the lens in SD-OCT. Even more so for the case if the iris was degenerated and not amenable to dilation by atropine. This was most likely the case for *Crybb2*<sup>O377/O377</sup> (Fig. 3, A, blue arrow) and *Crybb2*<sup>Philly/Philly</sup> (Fig. 3, E, blue arrow), where the iris did not dilate sufficiently.

### 5.2. Lens size

Another limitation for detecting the entire lens, independent of mice age and iris condition, was simply the lens size in relation to the already dilated pupil. Therefore, insights into the lens bow region were limited, e.g. in *Crygd*<sup>Aye4/Aye4</sup> (Fig. 1, F, black arrows) or more critical to acquire in the lens bow, densely populated with nuclei-containing fibre cells as in the *Crybb2*<sup>Aey2/Aey2</sup> mutant (Fig. 4, A, blue arrows). Likewise the vacuole-rich lesions of *Cryaa*<sup>Aey7/Aey7</sup> lenses were covered by the iris (Fig. 5, A, black arrow). Hence, histological analysis was necessary to garner information about the lens bow.

### 5.3. Mouse age

Also mouse age was a critical parameter for OCT imaging quality. Generally, older mice (e.g. *Ercc2*<sup>+/S737P</sup>, 18 months old) exhibited strong head movements due to extremely heavy breathing which rendered it barely possible to acquire more than 5-20 frames after standardisation in OCT mode. Therefore, OCT pictures of younger mice were much sharper and accurate. One possibility to accomplish a recording for older mice, is to fix their heads by the upper front teeth in a clamp.

### 5.4. Interferences

Other eye structures, e.g. the retina or the applied plan-convex contact lens could potentially interfere with OCT's of a chosen lens plane (Fig. 4, F, purple star). These overlays could be avoided by slightly increasing or decreasing the distance of the OCT reference arm slider and the camera focus respectively. Also enhanced depth imaging (EDI), adjustable in life mode, can help to cope with these problems.

Table 2: Potential capability of used methods for aberration detection in different lens regions.

		Method		
		Scheimpflug	Histology	OCT
Lens part	Anterior cortex	+	+	+
	Anterior c/n interface	+	–	+
	Nucleus	+	–	+
	Lens bow	–	+	–
	Posterior n/c interface	+	–	+
	Posterior cortex	–	+	+

Decisions, whether a method was appropriate based on inter-method comparisons. (c/n) Cortex to nucleus. (n/c) Nucleus to cortex. (–) Ambiguous detection. (+) Possible detection.

## 6. Conclusion

Altogether, the SD-OCT technique is easy to apply for detailed examination of the lens, in addition to the analysis of the retina. SD-OCT allows *in vivo* monitoring of developmental and pathological changes in the eye lens that occur from the anterior to the posterior end (Table 2). Especially the fine structure of nuclear alterations, that are untraceable in histology (due to imperfect fixation), were visible in SD-OCT (e.g. *Crybb2<sup>Aey2/Aey2</sup>*, *Crygd<sup>Aey4/Aey4</sup>* and *Cryba2<sup>Aca30/Aca30</sup>*). SD-OCT was also optimal for imaging features of the anterior lens which is considered as the main focus of Scheimpflug camera (e.g. *Crybb2<sup>+ /Aey11</sup>*). As a limitation, SD- and AS-OCT are not able to detect the lens bow, for which reason histology should be performed in addition. Also, up to now, there are no means to quantify lens opacifications within the Spectralis<sup>®</sup> software. On the other hand, the Pentacam<sup>®</sup> Scheimpflug device offers quantification tools, but is not able to detect posterior lens alterations.

Thus, SD-OCT imaging proves to be an excellent method for *in vivo* examinations in long-term studies with repeated measurements of the same mice and gives more detailed insights into the lens than other visualisation methods like Scheimpflug camera or slitlamp.

## Acknowledgments

We thank Erika Bürkle and Monika Stadler for the excellent technical assistance and Dr. Lillian Garrett for critical reading of the manuscript. The German Mouse Clinic received funding by the

German Federal Ministry of Education and Research (Infrafrontier grant 01KX1012 to MHdA). This study was partly financed by the LDLensRad project that received funding from the Euratom research and training programme 2014-2018 under grant agreement No 662287. This publication reflects only the author’s view. Responsibility for the information and views expressed therein lies entirely with the authors. The European Commission is not responsible for any use that may be made of the information it contains.

## Disclosure statement

The authors declare to have no potential conflicts of interest.

- Asrani, S., Sarunic, M., Santiago, C., Izatt, J., 2008. Detailed visualization of the anterior segment using Fourier-domain optical coherence tomography. *Arch Ophthalmol.* 126 (6), 765–771.
- Bermudez, M. A., Vicente, A. F., Romero, M. C., Arcos, M. D., Abalo, J. M., Gonzalez, F., 2011. Time course of cold cataract development in anesthetized mice. *Curr Eye Res.* 36 (3), 278–284.
- Chou, T.-H., Kocaoglu, O. P., Borja, D., Ruggeri, M., Uhlhorn, S. R., Manns, F., Porciatti, V., 2011. Postnatal elongation of eye size in DBA/2J mice compared with C57BL/6J mice: *in vivo* analysis with whole-eye OCT. *Invest Ophthalmol Vis Sci.* 52 (6), 3604–3612.
- Dalke, C., Neff, F., Bains, S. K., Bright, S., Lord, D., Graw, J., Reitmeir, P., Rößler, U., Samaga, D., Unger, K., Braselmann, H., et al., 2018. Lifetime study in mice after acute low-dose ionizing radiation: a multifactorial study with special focus on cataract risk. *Radiat Environ Biophys.* 57 (2), 99–113.
- de Castro, A., Benito, A., Manzanera, S., Mompeán, J., Canizares, B., Martínez, D., Marín, J. M., Grulkowski, I., Artal, P., 2018. Three-dimensional cataract crystalline lens imaging with swept-source optical coherence tomography. *Investigative ophthalmology & visual science* 59 (2), 897–903.

- Fukuda, S., Kawana, K., Yasuno, Y., Oshika, T., 2010. Repeatability and reproducibility of anterior ocular biometric measurements with 2-dimensional and 3-dimensional optical coherence tomography. *J Cataract Refract Surg.* 36 (11), 1867–1873.
- Ganguly, K., Favor, J., Neuhäuser-Klaus, A., Sandulache, R., Puk, O., Beckers, J., Horsch, M., Schädler, S., Vogt-Weisenhorn, D., Wurst, W., et al., 2008. Novel allele of *Crybb2* in the mouse and its expression in the brain. *Invest Ophthalmol Vis Sci.* 49 (4), 1533–1541.
- Graw, J., Löster, J., Puk, O., Münster, D., Haubst, N., Soewarto, D., Fuchs, H., Meyer, B., Nürnberg, P., Pretsch, W., et al., 2005. Three novel *Pax6* alleles in the mouse leading to the same small-eye phenotype caused by different consequences at target promoters. *Invest Ophthalmol Vis Sci.* 46 (12), 4671–4683.
- Graw, J., Löster, J., Soewarto, D., Fuchs, H., Meyer, B., Reis, A., Wolf, E., Balling, R., Hrabě de Angelis, M., 2001a. Characterization of a new, dominant V124E mutation in the mouse  $\alpha$ -crystallin-encoding gene. *Invest Ophthalmol Vis Sci.* 42 (12), 2909–2915.
- Graw, J., Löster, J., Soewarto, D., Fuchs, H., Reis, A., Wolf, E., Balling, R., Angelis, M., 2002. V76d mutation in a conserved  $\gamma$ -crystallin region leads to dominant cataracts in mice. *Mamm Genome.* 13 (8), 452–455.
- Graw, J., Löster, J., Soewarto, D., Fuchs, H., Reis, A., Wolf, E., Balling, R., Hrabě de Angelis, M., 2001b. *Aey2*, a new mutation in the  $\beta$ 2-crystallin-encoding gene of the mouse. *Invest Ophthalmol Vis Sci.* 42 (7), 1574–1580.
- Grułkowski, I., Manzanera, S., Cwiklinski, L., Mompeán, J., de Castro, A., Marin, J. M., Artal, P., 2018. Volumetric macro-and micro-scale assessment of crystalline lens opacities in cataract patients using long-depth-range swept source optical coherence tomography. *Biomedical optics express* 9 (8), 3821–3833.
- Huang, D., Swanson, E. A., Lin, C. P., Schuman, J. S., Stinson, W. G., Chang, W., Hee, M. R., Flotte, T., Gregory, K., Puliafito, C. A., et al., 1991. Optical coherence tomography. *Science.* 254 (5035), 1178–1181.
- Izatt, J. A., Boppart, S., Bouma, B., De Boer, J., Drexler, W., Li, X., Yasuno, Y., 2017. Introduction to the feature issue on the 25 year anniversary of optical coherence tomography. *Biomed Opt Express.* 8 (7), 3289–3291.
- Izatt, J. A., Hee, M. R., Swanson, E. A., Lin, C. P., Huang, D., Schuman, J. S., Puliafito, C. A., Fujimoto, J. G., 1994. Micrometer-scale resolution imaging of the anterior eye *in vivo* with optical coherence tomography. *Arch Ophthalmol.* 112 (12), 1584–1589.
- Kador, P. F., Fukui, H. N., Fukushi, S., Jernigan Jr, H. M., Kinoshita, J. H., 1980. Philly mouse: a new model of hereditary cataract. *Exp Eye Res.* 30 (1), 59–68.
- Kim, J.-S., Chung, S.-H., Joo, C.-K., 2009. Clinical application of a Scheimpflug system for lens density measurements in phacoemulsification. *J Cataract Refract Surg.* 35 (7), 1204–1209.
- Kunze, S., Dalke, C., Fuchs, H., Klaften, M., Rössler, U., Hornhardt, S., Gomolka, M., Puk, O., Sabrautzki, S., Kulka, U., et al., 2015. New mutation in the mouse *Xpd/Ercc2* gene leads to recessive cataracts. *PLoS One.* 10 (5), e0125304.
- Lavanya, R., Foster, P. J., Sakata, L. M., Friedman, D. S., Kashiwagi, K., Wong, T.-Y., Aung, H. T., Alfred, T., Gao, H., Ee, A. G., et al., 2008. Screening for narrow angles in the singapore population: evaluation of new noncontact screening methods. *Ophthalmology.* 115 (10), 1720–1727.
- Liu, J. J., Grułkowski, I., Kraus, M. F., Potsaid, B., Lu, C. D., Baumann, B., Duker, J. S., Hornegger, J., Fujimoto, J. G., 2013. *In vivo* imaging of the rodent eye with swept source/Fourier domain OCT. *Biomed Opt Express.* 4 (2), 351–363.
- Nolan, W. P., See, J. L., Chew, P. T., Friedman, D. S., Smith, S. D., Radhakrishnan, S., Zheng, C., Foster, P. J., Aung, T., 2007. Detection of primary angle closure using anterior segment optical coherence tomography in asian eyes. *Ophthalmology.* 114 (1), 33–39.
- Pei, X., Bao, Y., Chen, Y., Li, X., 2008. Correlation of lens density measured using the pentacam scheimpflug system with the lens opacities classification system iii grading score and visual acuity in age-related nuclear cataract. *Br J Ophthalmol.* 92 (11), 1471–1475.
- Puk, O., Ahmad, N., Wagner, S., Hrabě de Angelis, M., Graw, J., 2011. First mutation in the  $\beta$ a2-crystallin encoding gene is associated with small lenses and age-related cataracts. *Invest Ophthalmol Vis Sci.* 52 (5), 2571–2576.
- Puk, O., Dalke, C., Calzada-Wack, J., Ahmad, N., Klaften, M., Wagner, S., Hrabě de Angelis, M., Graw, J., 2009. Reduced corneal thickness and enlarged anterior chamber in a novel ColVIIIa2G257D mutant mouse. *Invest Ophthalmol Vis Sci.* 50 (12), 5653–5661.
- Puk, O., Hrabě de Angelis, M., Graw, J., 2013. Longitudinal fundus and retinal studies with SD-OCT: a comparison of five mouse inbred strains. *Mamm Genome.* 24 (5-6), 198–205.
- Radhakrishnan, S., Rollins, A. M., Roth, J. E., Yazdanfar, S., Westphal, V., Bardenstein, D. S., Izatt, J. A., 2001. Real-time optical coherence tomography of the anterior segment at 1310 nm. *Arch Ophthalmol.* 119 (8), 1179–1185.
- Swarup, A., Bell, B. A., Du, J., Han, J. Y., Soto, J., Abel, E. D., Bravo-Nuevo, A., FitzGerald, P. G., Peachey, N. S., Philp, N. J., 2018. Deletion of *glut1* in mouse lens epithelium leads to cataract formation. *Exp Eye Res.* 172, 45–53.
- Wegener, A., Laser-Junga, H., 2009. Photography of the anterior eye segment according to Scheimpflug's principle: options and limitations—a review. *Clin Exp Ophthalmol.* 37 (1), 144–154.
- Zhou, X., Xie, J., Shen, M., Wang, J., Jiang, L., Qu, J., Lu, F., 2008. Biometric measurement of the mouse eye using optical coherence tomography with focal plane advancement. *Vision Res.* 48 (9), 1137–1143.